Origin of energetic ions in the polar cusp inferred from ion composition measurements by the Viking satellite

G. Kremser[1,2], J. Woch[2], K. Mursula[1], P. Tanskanen[1], B. Wilken[2], R. Lundin[3]

[1] University of Oulu, Department of Physics, FIN-90570 Oulu, Finland
[2] Max-Planck-Institut für Aeronomie, D-37191 Katlenburg-Lindau, Germany
[3] Swedish Institute of Space Physics, S-98128 Kiruna, Sweden

Received: 6 June 1994/Revised: 4 November 1994/Accepted: 8 November 1994

Abstract. The magnetospheric ion composition spectrometer MICS on the Swedish Viking satellite provided measurements of the ion composition in the energy range 10.1 keV/e $\leq E/Q \leq$ 326.0 keV/e. Data obtained during orbit 842 were used to investigate the ion distribution in the northern polar cusp and its vicinity. The satellite traversed the outer ring current, boundary region, cusp proper and plasma mantle during its poleward movement. H^+ and He^{++} ions were encountered in all of these regions. He^+ ions were present only in the ring current. The number of O^+ and O^{++} ions was very small. Heavy high-charge state ions typical for the solar wind were observed for the first time, most of them in the poleward part of the boundary region and in the cusp proper. The H^+ ions exhibited two periods with high intensities. One of them, called the BR/CP event, appeared at energies up to 50 keV. It started at the equatorward limit of the boundary region and continued into the cusp proper. Energy spectra indicate a ring current origin for the BR/CP event. Pitch angle distributions show downward streaming of H^+ ions at its equatorward limit and upward streaming on the poleward side. This event is interpreted as the result of pitch angle scattering of ring current ions by fluctuations in the magnetopause current layer in combination with poleward convection. The other of the two periods with high H^+ ion intensities, called the accelerated ion event, was superimposed on the BR/CP event. It was restricted to energies $\leq$15 keV and occurred in the poleward part of the boundary region. This event is regarded as the high-energy tail of magnetosheath ions that were accelerated while penetrating into the magnetosphere. The cusp region thus contains ions of magnetospheric as well as of magnetosheath origin. The appearance of the ions depends, in addition to the ion source, on the magnetic field configuration and dynamic processes inside and close to the cusp.

Correspondence to: G. Kremser

1 Introduction

Particle observations play a key role in the investigation of the polar cusp. The cusp location is identified by the presence of typical energy-pitch angle dependent intensity variations of ions with energies in the keV range (see e.g. Burch *et al.*, 1982; Kremser and Lundin, 1990; Aparicio *et al.*, 1991). These variations are interpreted as transit time effects of magnetosheath plasma penetrating into the cusp under the influence of poleward convection (Burch *et al.*, 1982). It has been shown, furthermore, that the ion energy spectrum in the cusp resembles the magnetosheath ion spectrum (Newell and Meng, 1988; Woch and Lundin, 1992). The maximum ion number density in the cusp agrees with that expected for the shocked plasma in the magnetosheath above the cusp regions (Aparicio *et al.*, 1991). Amundsen *et al.* (1975) observed a high-energy tail in the proton energy spectrum together with magnetosheath-like plasma. The magnetosheath plasma penetrates either directly into the magnetosphere as it does in the cusp proper, or in association with acceleration processes as in the adjacent boundary region (Woch and Lundin, 1992). The plasma can propagate deeply into the magnetosphere and generate modifications of the ionosphere (Watermann *et al.*, 1994). The magnetosheath can therefore be regarded as a well-established particle source.

Ionospheric particles have also been observed in the cusp and in the region adjacent to it. Viking measurements show that they appear as beams or conics with ion energies up to a few keV (Thelin *et al.*, 1990) that result from ion acceleration by the interaction with broadband low-frequency waves (André *et al.*, 1988; 1990) or Alfvén waves (Peterson *et al.*, 1993). Upwelling of ions at much lower energies has been reported by Lockwood *et al.* (1985), Winglee *et al.* (1993), and many others. Upflowing has been investigated e.g. by Yau *et al.* (1984). These ions may constitute an important source for the ring current (Delcourt *et al.*, 1990). The acceleration of ionospheric electrons to energies up to about 10 keV in the boundary region adjacent to the cusp was reported by Kremser and Lundin (1990).

Another possible particle source is the magnetosphere. The cusp is located on magnetic field lines adjacent to magnetospheric regions like the ring current or the plasma sheet. Particles may diffuse or be scattered from these regions into the cusp. Magnetospheric particles may also enter the cusp via the low-latitude boundary layer. In general, magnetospheric particles have higher energies than magnetosheath particles. The energy ranges overlap, however, at energies of several keV. Kremser and Lundin (1990) investigated particle measurements in this transitory energy range. They realized that magnetospheric particles are present in the cusp region in addition to magnetosheath particles. They used data from an instrument that allowed a distinction to be made between H^+ and He^{++} ions, but the count rates of the instrument were so low that data from many cusp crossings had to be superimposed in a statistical study.

Detailed analysis of data obtained by the ion composition spectrometer MICS on the Swedish Viking satellite provides new information on the origin of energetic ions in the cusp region. The MICS instrument is described in an appendix to this paper together with the method of data analysis. MICS filters ions with equal value of the energy per charge state E/Q and measures their time-of-flight τ and residual energy E_m. These parameters are then used to determine the ion mass M in amu, charge state Q, and energy E. The energy range of the instrument extends from 10.1 to 326.0 keV/e. The Viking orbit had an apogee height of 13530 km, a perigee height of 817 km, an inclination of 98.8°, and an orbital period of 262 min. The satellite carried a combination of particle, field, and wave instruments as well as an auroral imager for the investigation of high-latitude midaltitude magnetospheric processes (Hultqvist, 1987, 1990). Viking frequently traversed the northern polar cusp.

MICS data were used to investigate the ion composition in the polar cusp during orbit 842. They represent the first observations of energetic heavy ions with high charge states like O^{6+}, C^{6+} as well as Mg, Si, and Ca ions in the cusp, definitely proving their magnetosheath origin. On the other hand H^+ ions were observed that are very likely scattered from the ring current by the interaction with the magnetopause current layer. An additional component to these ions is provided by the acceleration of magnetosheath ions. The observations thus show that the energetic ion population in the cusp region comprises ions originating from the magnetosheath as well as from the magnetosphere. The appearance of these ions depends on the magnetic field configuration and is influenced by dynamic processes inside and close to the cusp.

2 Observations

2.1 Event structure: hot plasma observations

We selected Viking orbit 842 on 24 July 1986. According to Woch and Lundin (1992) the interplanetary magnetic field had a strong southward and a considerable dawnward component during this event. The geomagnetic field was disturbed, with $K_p = 6$. The satellite traversed the cusp in the poleward direction at an altitude of about 13500 km. Figure 1 displays a section of the satellite trajectory in magnetic local time MLT and invariant latitude ILAT. We included the division of the observation period (2219–2243 UT) into the ring current, boundary region, cusp proper, and plasma mantle. The corresponding time intervals are listed in Table 1.

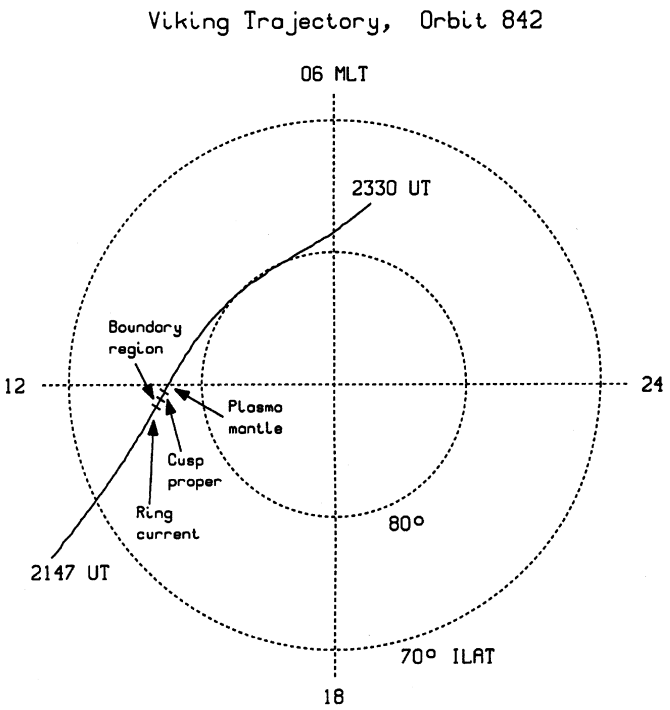

Fig. 1. A section of the Viking trajectory during orbit 842 in magnetic local time (MLT) and invariant latitude (ILAT) coordinates. The division into ring current, boundary region, cusp proper and plasma mantle is explained in the text. See also Fig. 2 and Table 1

Table 1. Division of the observation period

Section	Time interval, UT
Ring current	until 2231:20
Boundary region I	2231:20–2232:00
Boundary tegion II	2232:00–2233:15
Cusp proper	2233:15–2235:15
Plasma mantle	from 2235:15 onwards

The division is based on the work by Woch and Lundin (1992), who investigated time-energy spectrograms of electrons and ions using data from the hot plasma experiment package on Viking (Sandahl *et al.*, 1985). The spectrograms for orbit 842 are displayed in the upper part of Fig. 2. The ring current ions appear as intensity maximum at energies around 10 keV. This interval is indicated by "RC" in a panel just below the spectrograms.

The boundary region (BR) "is characterized by an isotropization and flux decrease of the ring current population and by a structured low-energy population and upward moving ions" (Woch and Lundin, 1992). In this case, the upward moving ions appear as conics. In addition,

Viking Orbit 842 24 July, 1986

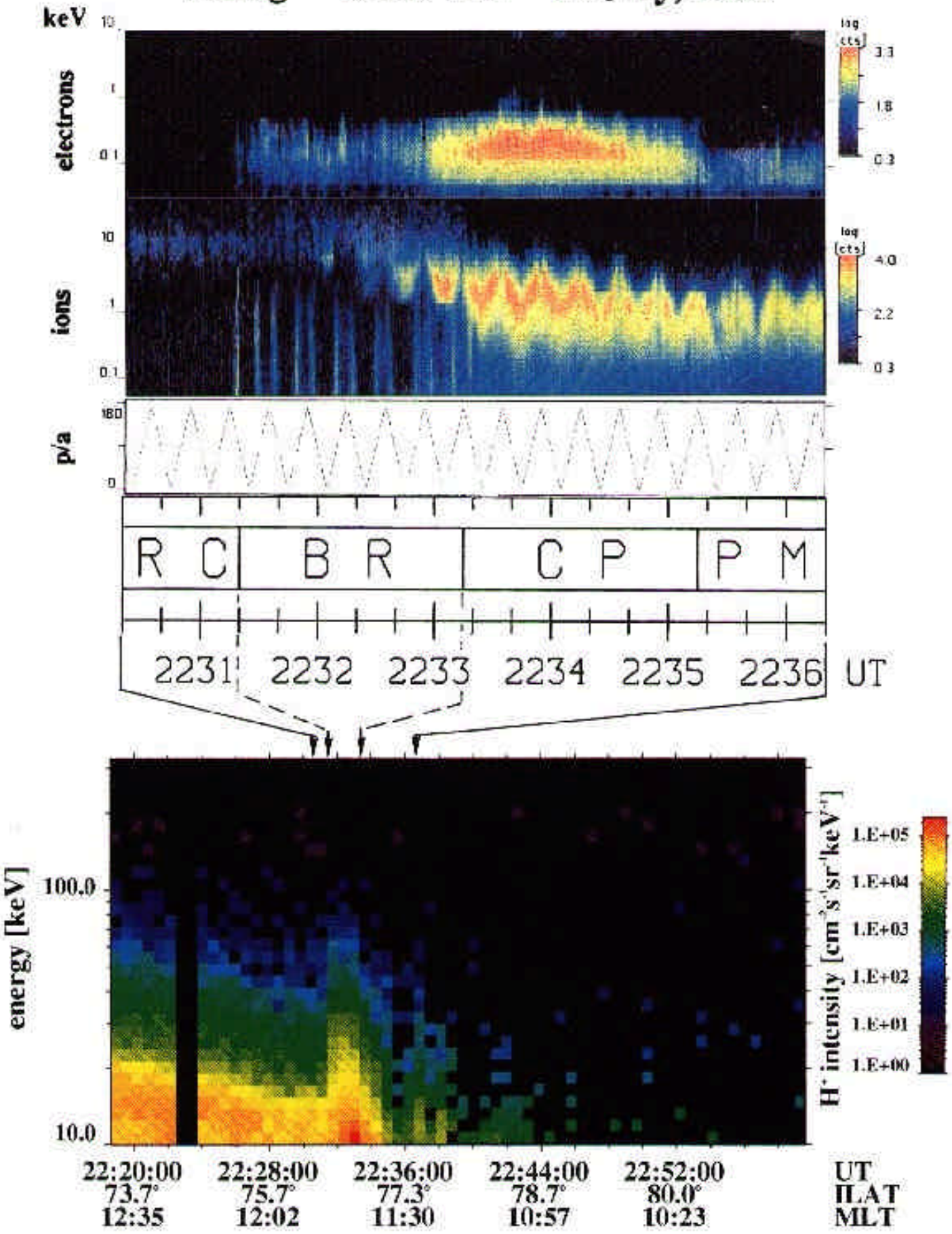

Fig. 2. Upper part: Energy-time spectrograms of electrons (panel 1) and ions (panel 2) according to measurements with the hot plasma experiment package on Viking. The third panel, labelled p/a, displays the pitch angles. The fourth panel indicates the division of the observation period into ring current (RC), boundary region (BR), cusp proper (CP), and plasma mantle (PM). Lower part: Energy-time spectrograms of H^+ ions according to MICS observations

accelerated magnetosheath ions are present. They are seen at energies above the ion energies in the subsequent cusp proper (CP). Note also the relatively high ion intensities at energies above the intensity maximum in the ring current. This ion population is one of the main subjects of our investigation (called BR/CP event in the next section).

We subdivided the boundary region into two parts. The first part, called 'boundary region I' precedes the appearance of accelerated magnetosheath ions, whereas the second part, the 'boundary region II' includes them. As will be shown below in the discussion of MICS data, significant differences in the energetic ion populations were encountered within these two parts of the boundary region.

In the CP, the ions exhibit characteristic pitch angle-energy dependent intensity variations at energies up to a few keV, whereas an almost structureless electron population is present at energies of about 100 eV. The pitch angle and energy dependent ion intensity variations continue in the plasma mantle (PM), but the electron intensity is much smaller in this region than in the CP.

2.2 *MICS data overview: variations of the H^+ ion intensity*

The lower part of Fig. 2 displays a spectrogram of the H^+ ion intensity as it was measured by the MICS instrument. The first part of it shows how the H^+ ion intensity decreases with increasing latitude in the ring current. This decrease is interrupted by an abrupt intensity increase as the satellite enters the BR. The period with high intensities continues into the cusp proper, but ends before the satellite reaches the poleward boundary of the cusp.

The same data are displayed as histograms in Fig. 3 to demonstrate further details. We have repeated at the top the division into the ring current, BR, CP and plasma mantle. The poleward traversal of the high-latitude ring current, characterized by decreasing intensities, continues until 2231:20 UT. The superimposed intensity fluctuations are due to statistical uncertainties and pitch angle variations and are therefore not significant.

At the onset of the subsequent time interval from 2231:20 to 2234:20 UT, the intensity rises sharply, first at energies above 25 keV and during the following 20-s time bin also at lower energies. Since this period is related to the entrance of the satellite into the BR and continues into the CP, we designate this part of the observations as the 'BR/CP event'. Its duration is indicated by a bar at the top of Fig. 3.

An additional intensity increase is superimposed on the BR/CP event in the two lowermost energy channels between 2232:40 and 2233:40 UT. It is somewhat difficult to recognize this event in Fig. 3, because of relatively strong intensity fluctuations of other origins. Further evidence for its existence will be presented below, e.g. in the discussion of the energy spectra in Fig. 6b and c. This increase occurred close to the poleward limit of the BR, i.e. within the acceleration region of solar wind origin ions observed by Woch and Lundin (1992). We therefore call it the 'accelerated ion event' (AIE) in this paper. Its duration is also indicated by a bar at the top of Fig. 3.

The intensity decreases to very low values after 2234:20 UT and is then most of the time below the sensitivity level of the instrument. This part covers the poleward part of the CP and the plasma mantle.

In the following we focus the investigations on the BR/CP and AIE events that occurred between 2231:20 and 2235:15 UT.

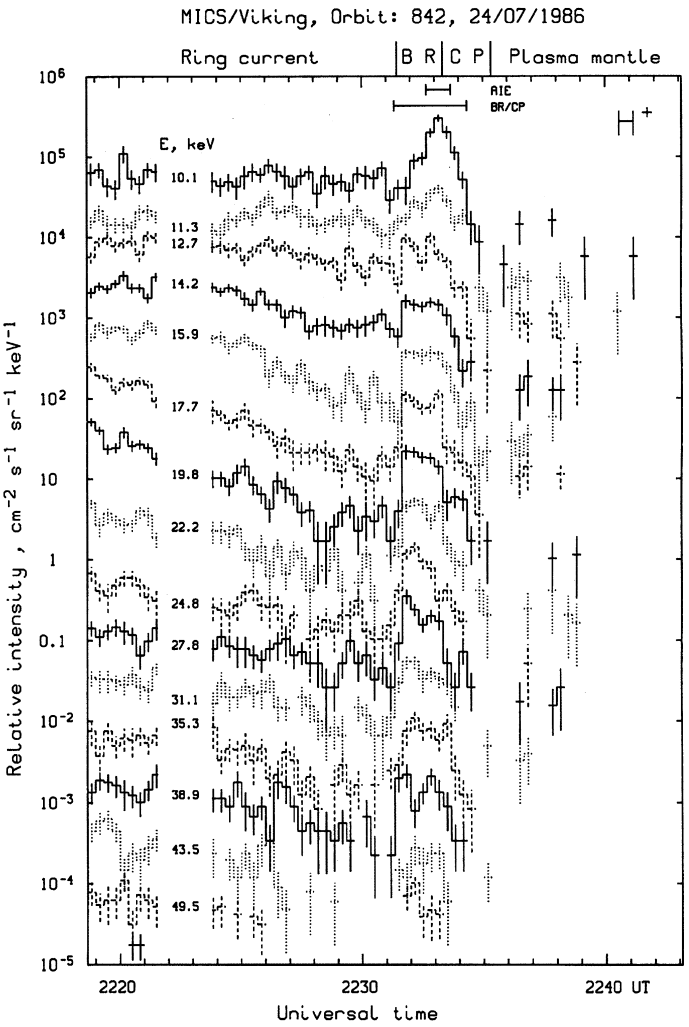

Fig. 3. Temporal variations of the H^+ ion intensity in the pitch angle range 20°–160° according to MICS observations. The numbers on the left-hand side indicate the ion energy. The abbreviations BR and CP on the topside correspond to boundary region and cusp proper, respectively. *Horizontal bars* indicate the durations of the BR/CP event and the accelerated ion event (AIE). Relative intensities were introduced to avoid overlaps in the plotting of the intensities in the different energy channels. Their values were obtained by multiplying the intensities with the following factors: 1.0 (10.1 keV), 0.32 (11.3 keV), 0.1 (12.7 keV), $3.2 \cdot 10^{-2}$ (14.2 keV), 10^{-2} (15.9 keV), $3.2 \cdot 10^{-3}$ (17.7 keV), 10^{-3} (19.8 keV), $3.2 \cdot 10^{-4}$ (22.2 keV), 10^{-4} (24.8 keV), $3.2 \cdot 10^{-5}$ (27.8 keV), 10^{-5} (31.1 keV), $3.2 \cdot 10^{-6}$ (35.3 keV), 10^{-6} (38.9 keV), $3.2 \cdot 10^{-7}$ (43.5 keV), 10^{-7} (49.5 keV)

2.3 *Ion composition*

Results of the ion identification procedure explained in the appendix are shown in Fig. 4a–e. The + sign, the letters O and X, and the numbers 1 and 2 indicate ions identified by their mass M and charge state Q. The dots represent ions, for which only M/Q could be determined. Each figure represents the ion composition in one of the regions, into which the total measurement period was divided according to the hot plasma data.

H^+ is the most abundant ion species in all regions, as is indicated by the number of + signs and the dots close to the $M/Q = 1$ curve.

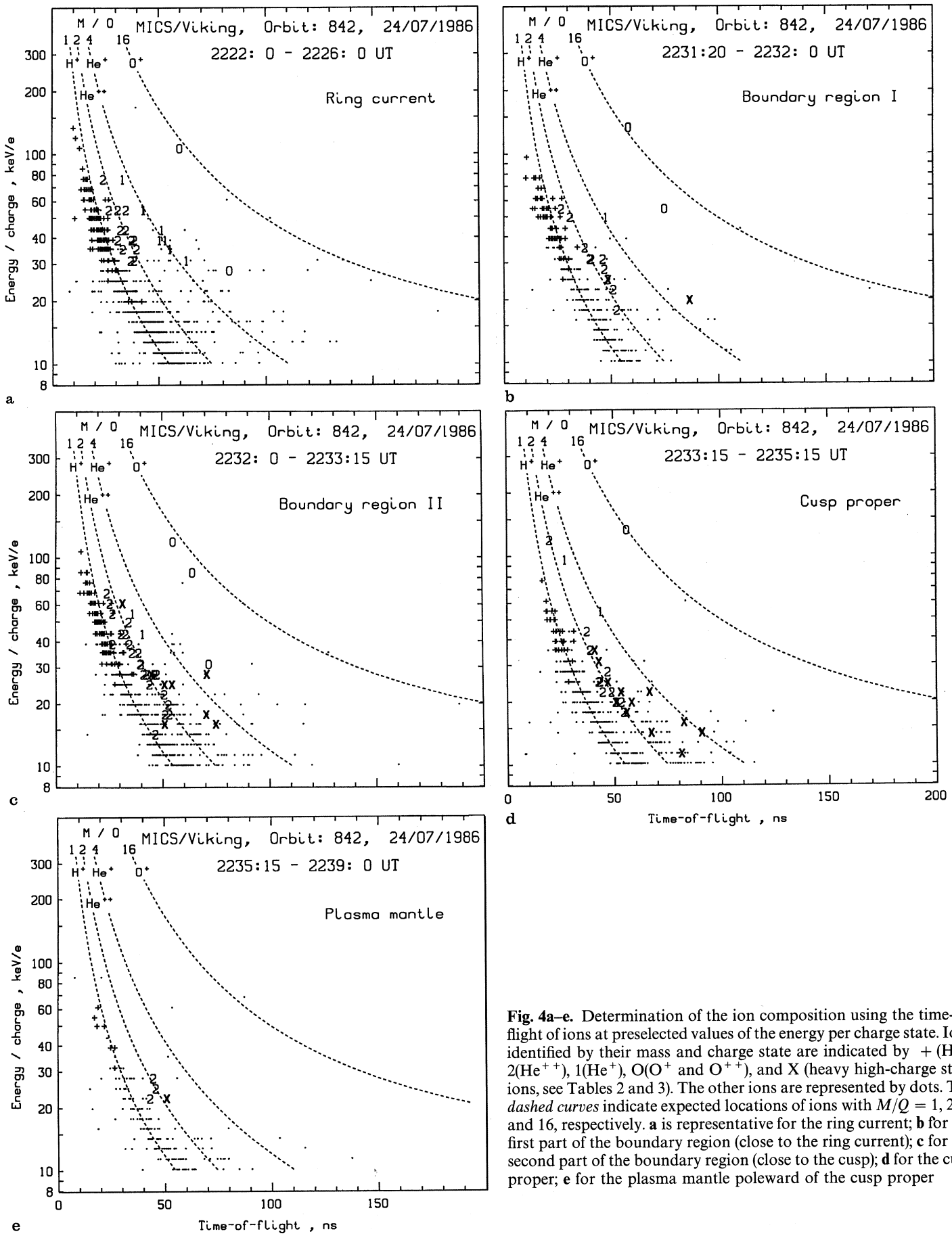

Fig. 4a–e. Determination of the ion composition using the time-of-flight of ions at preselected values of the energy per charge state. Ions identified by their mass and charge state are indicated by $+ (H^+)$, $2(He^{++})$, $1(He^+)$, $O(O^+$ and $O^{++})$, and X (heavy high-charge state ions, see Tables 2 and 3). The other ions are represented by dots. The *dashed curves* indicate expected locations of ions with $M/Q = 1, 2, 4$, and 16, respectively. **a** is representative for the ring current; **b** for the first part of the boundary region (close to the ring current); **c** for the second part of the boundary region (close to the cusp); **d** for the cusp proper; **e** for the plasma mantle poleward of the cusp proper

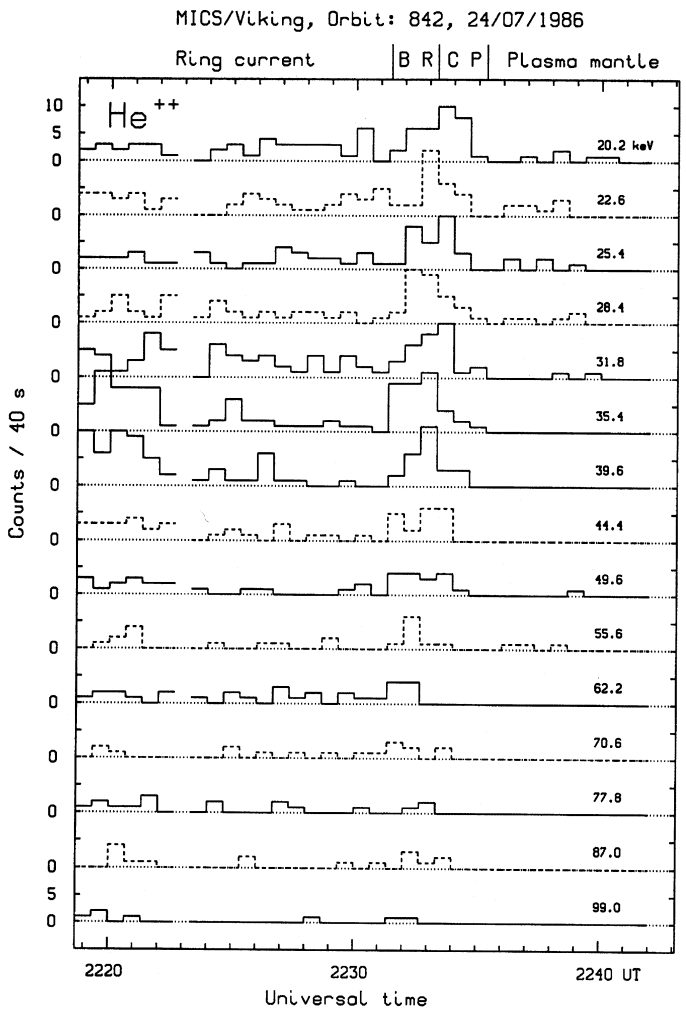

Fig. 5. Count rates of He^{++} ions transmitted as direct event data DE (see appendix). BR is the boundary region, CP the cusp proper. The numbers on the right-hand side indicate the ion energy

He^{++} ions are also present in all regions. They are indicated by a 2 or by dots close to the $M/Q = 2$ curve. Note, however, an important energy dependence of these ions. Most of the He^{++} ions in the ring current are restricted to energies above 30 keV/e, whereas the energy limit decreases to 20 keV/e in the BR and to even lower values in the CP. A comparison of Fig. 4a with Fig. 4d shows the much larger number of dots in the lowermost energy channel close to the $M/Q = 2$ curve in the CP as compared to the ring current. This increase corresponds to a large flux of He^{++} ions, since the sensitivity of the instrument decreases strongly with decreasing energy due to ion scattering and energy losses in the carbon foil of the time-of-flight spectrometer (Stüdemann and Wilken, 1982).

The number of counts identified as He^{++} ions are plotted versus time in Fig. 5. In spite of strong statistical uncertainties, one can well recognize the high count rates in the ring current at energies between about 30 and 40 keV. The count rates also increase in the BR, showing that the He^{++} ion flux changed in a similar way with latitude as the H^+ ion flux (see Fig. 3), but the data are not adequate for a quantitative confirmation of this relationship.

He^+ ions (indicated by 1) are clearly present in the ring current (Fig. 4a), but their number is small as compared to the number of H^+ and He^{++} ions. They appear to be virtually absent outside the ring current (Fig. 4b–e). The number of O^+ and O^{++} ions (represented by O in Fig. 4a–e) is very small, indicating a lack of these ions in the cusp region as well as in the high-latitude part of the outer ring current.

Special attention should be paid to the ions indicated in Fig. 4b–e by the letter *X*. It indicates the presence of heavy high-charge state ions. Most of them appeared in BR II and the CP. An unambiguous identification of these ions is difficult, since the ions suffer considerable energy losses in the carbon foil and in the front dead layer of the solid-state detector of the time-of-flight spectrometer. As explained in the appendix, we could reliably identify the carbon and oxygen ions listed in Table 2, but the ions heavier than oxygen listed in Table 3 could only be identified in a tentative way. For these ions, the energy (E_{corr}), mass (M), and charge state (Q) were calculated using model calculations for the energy losses of argon. It is clear, however, that the ion masses are well above the mass of helium ions and the charge states are higher than 4. Most of the ions have energies above 100 keV. They were observed in a wide range of pitch angles (column PA in Tables 2 and 3). The total number of 27 ions is large compared to the observation of high-charge state carbon and oxygen ions inside the magnetosphere by Kremser *et al.* (1987), who reported average count rates of about one per hour by a similar instrument (CHEM) on the AMPTE/CCE satellite. Note that the number of heavy high-charge state ions is also much larger than the number of O^+ ions.

2.4 Details of the H^+ ion distribution

2.4.1 Energy spectra. Average energy spectra of H^+ ions are displayed in Fig. 6a–c. The averaging includes all pitch angles, since the H^+ ion intensity is isotropic during most of the observation period (no figure). Figure 6a shows that the energy spectrum in the first part of the boundary region resembles the energy spectrum in the ring current for the time interval 2222–2226 UT (well before the entrance of the satellite into the BR). The energy spectra in the two parts of the BR are also very similar to each other apart from the two lowermost energy channels, in which the intensity is larger in part II than in part I (Fig. 6b). This difference is obviously related to the accelerated ion event (AIE) at the limit between BR II and CP. It shows that the intensity increase associated with this event is limited to energies below about 15 keV.

A comparison of the energy spectra in BR II with those obtained in the regions poleward of it (Fig. 6c) demonstrates a continuous intensity decrease with increasing invariant latitude, but only minor changes of the spectral shape. The AIE may still be present in the cusp proper, but not in the plasma mantle.

2.4.2 Streaming of H^+ ions. Two periods with anisotropic pitch angle distributions were encountered during

Table 2. Identification of high-charge state carbon and oxygen ions

Time, UT	E/Q, keV/e	M/Q_{obs}	E_{corr}, keV	M, amu	Q	Species	PA,°
Ring current							
2226:55	24.8	3.7	102	13.5	4.1	O^{4+}	138
2228:35	15.9	3.0	83	13.4	5.2	O^{5+}	134
2229:33	15.9	2.7	78	10.6	4.9	C^{5+}	80
Boundary region I							
2231:53	24.8	2.5	149	13.8	6.0	O^{6+}	51
Boundary region II							
2232:12	24.8	2.8	131	13.1	5.3	O^{6+}	35
2232:35	60.8	2.6	305	12.5	5.0	C^{5+}	85
2232:38	27.8	2.4	136	10.8	4.9	C^{5+}	109
2232:46	24.8	3.1	122	13.7	4.9	O^{5+}	88
2232:50	15.9	1.8	110	11.0	6.9	C^{6+}	11
Cusp proper							
2233:16	19.8	2.2	101	10.0	5.1	C^{6+}	101
2233:34	24.8	2.4	119	10.2	4.8	C^{5+}	52
2233:36	19.8	2.9	131	16.2	6.6	O^{6+}	84
2233:46	17.7	2.4	82	9.6	4.7	C^{5+}	99
2233:57	31.1	2.5	154	11.2	4.9	C^{5+}	109
Plasma mantle							
2236:55	22.2	2.5	110	11.0	4.9	C^{5+}	41

Table 3. Tentative identification of ions heavier than oxygen

Time, UT	E/Q, keV/e	M/Q_{obs}	E_{corr}, keV	M, amu	Q	Species	PA,°
Ring current							
2230:14	14.2	3.1	102	28	7.2	Si^{8+}	86
Boundary region I							
2231:26	19.8	6.3	192	53	9.7	Fe^{10+}	74
Boundary region II							
2232:39	17.7	3.7	131	22	7.4	Mg^{8+}	142
2233:07	27.8	5.9	168	30	6.1	Si^{7+}	76
2233:09	15.9	3.8	104	19	6.6	Na^{8+}	26
Cusp proper							
2233:19	15.9	4.6	144	34	9.1	Ca^{9+}	146
2233:29	11.3	3.2	104	22	9.2	Mg^{9+}	42
2233:36	14.2	5.0	118	32	8.3	Ca^{9+}	88
2233:38	22.2	4.2	214	36	9.6	Ca^{10+}	126
2233:38	22.2	2.7	236	25	10.6	Mg^{10+}	127
2234:00	14.2	2.7	157	25	11.0	Mg^{10+}	156
2234:00	35.3	2.6	473	33	13.4	Mg^{10+}	163

the BR/CP event. The energy spectra in Fig. 7 illustrate this anisotropy in detail. It appears at energies below about 30 keV. At the onset of the BR/CP event (Fig. 7a), in BR I, the intensity is larger for pitch angles $\leq 80°$ than for larger pitch angles. Later on, in the CP, the intensity is larger for pitch angles $\geq 100°$ than for smaller pitch angles (Fig. 7c). In between (Fig. 7b), the ion intensity is isotropic. Note that the period of isotropic intensities is the one during which the AIE event appears (see also Fig. 3).

The anisotropy indicates a net downward streaming of H^+ ions in the equatorward part of the BR/CP event (BR I) and a net upward streaming in its poleward part (CP). The downward streaming is associated with an intensity increase, the upward streaming with an intensity decrease.

2.5 Summary of observations

The temporal variations of the H^+ ion intensity in Figs. 2 and 3 show that Viking observed a strong intensity increase at $E < 50$ keV when it entered the boundary region poleward of the ring current (BR/CP event). The intensity remains high until the cusp proper in which it decreases to levels below the sensitivity of the MICS instrument. An additional intensity increase, restricted to $E < 15$ keV, was observed in BR II on the equatorward side of the CP (AIE). Variations of the He^{++} ion count rates indicate a similar behaviour for these ions (Fig. 5).

The observations of the ion composition, energy spectra, and pitch angle distributions are summarized in Table 4. The times in the first column indicate the lengths of the observation periods in the different regions. H^+ and

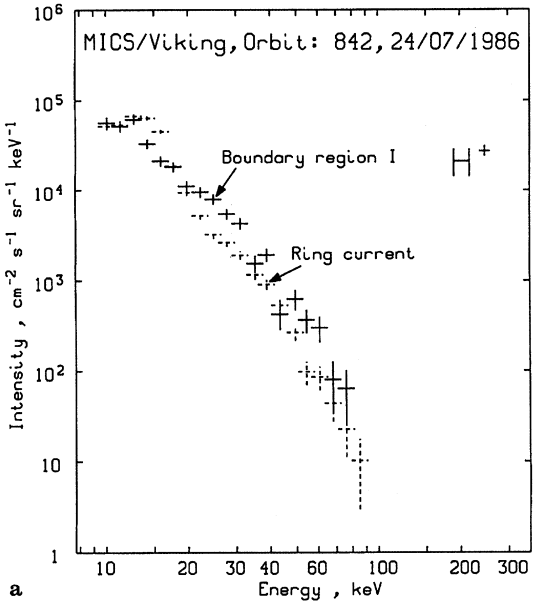

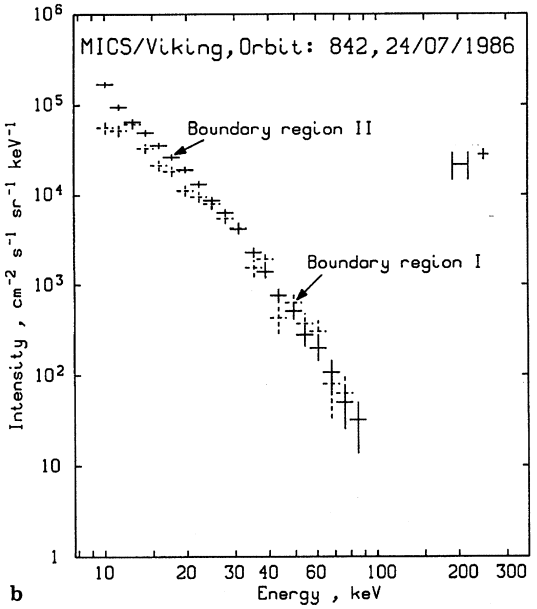

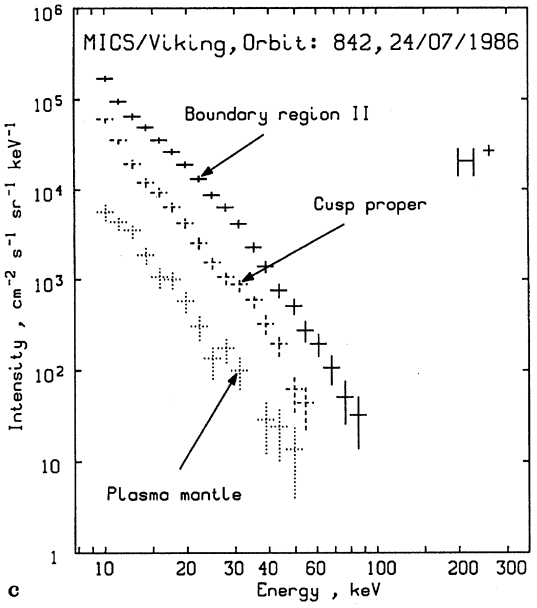

He^{++} ions were observed in all regions. Note, however, the decrease of the minimum He^{++} ion energy with increasing latitude. Heavy high-charge state ions were mainly present in BR II and the CP.

The shape of the energy spectrum in the BR resembles the spectrum in the ring current for high energies (>15 keV). At $E < 15$ keV, the intensity is larger in BR II than in the ring current, indicating an additional source for these ions.

The pitch angle distribution is generally isotropic. The intensity increase and decrease associated with the BR/CP event are anisotropic, however. During the increase a net downward streaming was observed at $E < 30$ keV. During the intensity decrease, the streaming was directed upward.

3 Interpretation

For the interpretation of the data, we assume that the magnetosheath and the magnetosphere are possible sources of energetic ions. The energy range of the MICS instrument is too high for the detection of possible ionospheric contributions. The main aim of our interpretation is therefore to evaluate, what parts of the observed ion populations may originate from the magnetosheath and the magnetosphere, respectively, and how the appearance of the ions depends on dynamic processes and the magnetic field configuration.

3.1 Ions from the magnetosheath

The observations show that heavy high-charge state ions, He^{++} ions at energies below 25 keV, and high H^+ ion intensities at energies below 15 keV (AIE) were present in boundary region II and the cusp proper.

The heavy high-charge state ions can only originate from the shocked solar wind in the magnetosheath. It was already mentioned in the section on observations that their number is by far too high for a magnetospheric origin. The ions can have been accelerated to the relatively high energies of more than 100 keV by an interaction with the bowshock (see e.g., Anagnostopoulos and Kaliabetsos, 1994). Heavy high-charge state ions with lower energies may also have been present, but could not be detected by the MICS instrument, since the electrostatic analyser restricts the energy range to $E/Q > 10$ keV/e.

The low-energy He^{++} ions ($E < 25$ keV) are very likely of solar wind origin. The ring current can be excluded as an alternative particle source, since the number of He^{++} ions with low energies in the ring current and even in BRI

Fig. 6a–c. Energy spectra of the H^+ ion intensity. **a** compares the spectra in the ring current and boundary region I, **b** in the two parts of the boundary region, and **c** in boundary region II, cusp proper, and plasma mantle. The ring current data were averaged over the time interval 2222–2226 UT, the plasma mantle data over 2235: 15–2239:00 UT, and the other data over the time intervals listed in Table 1

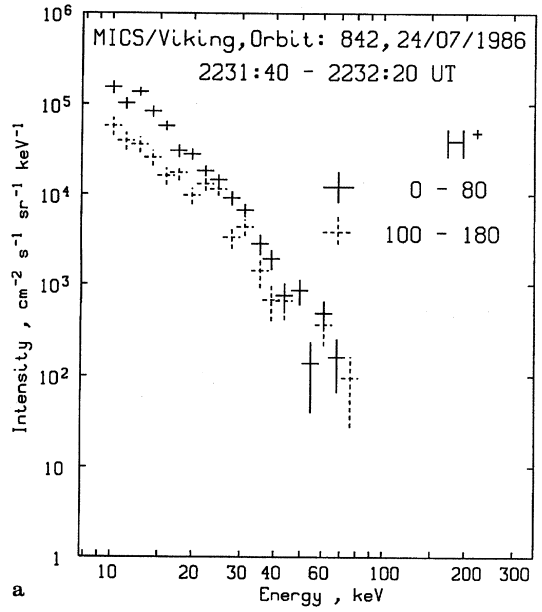

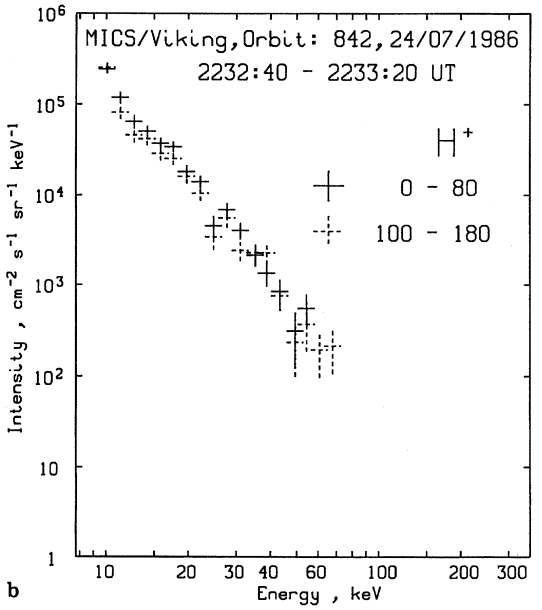

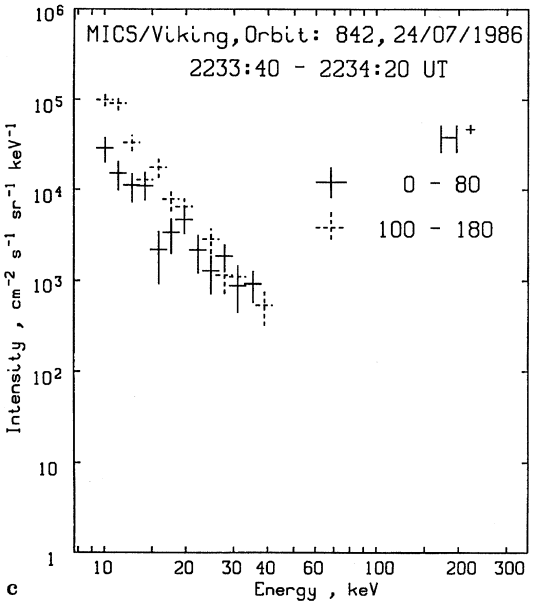

are considerably smaller than in BR II and the CP. Note also that the observed count rate increase at low energies corresponds to a large increase of the ion flux, since the sensitivity of MICS is low at these energies as was already explained in Sect. 2.3.

The protons with energies below 15 keV in the AIE can also be regarded to be of magnetosheath origin. This interpretation is corroborated by observations with the hot plasma experiment package on Viking, from which Woch and Lundin (1992) inferred an acceleration of magnetosheath origin plasma during the same event. It could be shown by these authors that the bulk of the magnetosheath ion distribution is accelerated by about 1 keV as compared to the ambient magnetosheath plasma. The acceleration is attributed to dayside merging. We therefore regard the increase in the proton intensities in the low-energy channels of the MICS instrument as the high-energy tail of the magnetosheath particles being affected by the same merging process, although we do not know any details about the corresponding acceleration process itself.

3.2 Ions from the magnetosphere

The H^+ ion intensities observed during the BR/CP event are much larger than in the adjacent parts of the ring current. The energies (up to 50 keV) at which the increase appeared are higher than the upper energy limit (15 keV) for the AIE. We therefore exclude a magnetosheath origin for the particles in the BR/CP event and regard a magnetospheric source as the more likely alternative.

The presence of magnetospheric particles in the boundary region and cusp proper can be explained by pitch angle scattering of ions in the outermost parts of the ring current. In the undisturbed situation, ions with equatorial pitch angles up to about 7° reach the Viking satellite during their bounce motion. However, if pitch angle scattering occurs, ions with larger pitch angles, i.e. also with higher intensities can reach the satellite and give rise to the observed intensity increase. The most likely scattering mechanism is the interaction with the magnetopause current layer. Fluctuations of this current layer are known to produce efficient pitch angle scattering (e.g. Lyons *et al.*, 1987).

The ions are scattered within a region inside the magnetosphere that has a maximum width of $2r_g$ (r_g is the ion gyro radius), i.e., the width depends on the ion energy. The observations (Figs. 2 and 3) indicate, in fact, that the intensity of the scattered ions first increases at high energies.

Fig. 7a–c. Energy spectra of H^+ ions in two pitch angle ranges for three selected 40-s intervals in the boundary region and cusp proper, indicating a transition from **a** asymmetric pitch angle distributions with higher intensities at pitch angles $\leq 80°$, to **b** isotropic distributions, and **c** to asymmetric distributions with higher intensities at pitch angles $\geq 100°$

Table 4. Summary of observations

Section	Ion composition	Energy spectrum	Pitch angle distribution
Boundary region I (40 s)	H^+, He^{++} (>35 keV), 2 high-charge state ions	Similar to ring current	$E \leq 30$ keV: $j(\geq 90°) > j(\leq 90°)$, $E \geq 30$ keV: isotropy
Boundary region II (75 s)	H^+, He^{++} (>25 keV), 8 high-charge state ions	$E \leq 15$ keV: j high; $E \geq 15$ keV: as ring current	Isotropy
Cusp proper (120 s)	H^+, He^{++} (>20 keV), 12 high-charge state ions	Shape as in BR II, j lower	$E \leq 30$ keV: $j(\geq 90°) < j(\leq 90°)$, $E \geq 30$ keV: isotropy
Plasma mantle (225 s)	H^+, He^{++} (>20 keV) 1 high-charge state ion	Shape as in BR I, j lower	Isotropy

Further evidence for ion scattering is provided by the observation of ion streaming that is directed downward during the intensity increase and upward during the decrease. The scattered ions move along the magnetic field lines to the satellite and further earthward to their mirror point. During this movement, they are subject to convection, if an electric field is present. The convection is most efficient close to the mirror points, since the ions spend most of their bounce period in the mirroring region, where the parallel velocity component is small. In our case, poleward convection existed (Woch and Lundin, 1992). Consequently, the mirrored ions move upward on field lines poleward of those on which they came down from the equator. If the convection is strong enough, the returning ions move more than a gyro radius away from the satellite. At the equatorward limit of the scattering region, one then only sees the downcoming ions. That explains the downward streaming in BR I during the intensity increase. The scattering stops, once the satellite has reached open field lines during its poleward movement but ions returning from their mirror point under the influence of convection may still be present. Upward streaming of scattered ions is therefore observed in this region.

A rough numerical estimate shows that the bounce period is several minutes. The poleward convection is approximately $10\ km\ s^{-1}$ relative to the satellite (Woch and Lundin, 1992). If we assume that it is most effective during about one third of the bounce period, the poleward movement due to convection amounts to several hundred km, whereas the gyro radius is smaller than 100 km. This means that poleward convection can in fact separate downcoming and upgoing ions from each other and thus explain the observed streaming. Downcoming and upgoing ions can be encountered together between the regions of streaming, where no anisotropy is observed.

Stadsnes (1988) already invoked a similar process to explain the presence of O^+ ions poleward of the limit for H^+ ions. We regard it as the most likely but not as the only possible mechanism to produce the BR/CP event. A stochastic interaction of magnetospheric particles with the magnetopause current layer may also produce energetic particles (see e.g. Lyons *et al.*, 1987). Convection of these particles can then give rise to the BR/CP event as well.

3.3 Magnetic field configuration

The interpretation of the BR/CP event in terms of pitch angle scattering of ring current ions implies that this event started on closed field lines just inside the magnetopause. Closed field lines were very likely present throughout the whole BR I, since the massive increase of magnetosheath ions starts in BR II only. The continuation of the BR/CP event poleward of BR I can be due to the poleward convection of these ions. The observations indicate indeed that they were present even in the CP.

The presence of magnetosheath ions in BR II indicates open field lines. It is difficult, however, to determine the exact limit between open and closed field lines from particle observations, since on the one hand magnetospheric ions can convect from closed field lines onto open field lines and on the other hand magnetosheath ions may be scattered from open field lines onto closed field lines. We think that the limit was located at the transition between the two parts of the BR or inside BR II.

It is not possible to distinguish between the crossing of a quasi-steady state boundary between open and closed field lines and a more dynamic situation in which field lines were just opened when the satellite crossed this region or in which the boundary between open and closed field lines moved across the satellite. The period of observation lasts a few minutes. This is comparable to the bounce periods as well as to other possible time constants involved like e.g. the repetition rate of flux transfer events (Lockwood and Smith, 1992). The fact that the geomagnetic field was disturbed during the event may favour a dynamic interpretation of the observations but no well founded conclusion on this point is possible from our data set.

Appendix A: Instrument and data analysis

MICS/Viking is a magnetospheric ion composition spectrometer flown on the Swedish satellite Viking. It is designated as V3-7 in the terminology of the Viking project. The instrument was briefly described by Stüdemann *et al.* (1987) and Rasinkangas *et al.* (1991). A similar spectrometer was included in the payload of the combined release

Table 5. Energy channels of MICS/Viking in keV/e

Channel	E/Q	Channel	E/Q	Channel	E/Q	Channel	E/Q
1	10.1	9	24.8	17	60.8	25	149.0
2	11.3	10	27.8	18	68.0	26	167.0
3	12.7	11	31.1	19	76.1	27	184.0
4	14.2	12	35.3	20	85.1	28	209.0
5	15.9	13	38.9	21	96.0	29	233.0
6	17.7	14	43.5	22	106.5	30	261.0
7	19.8	15	49.5	23	119.1	31	285.0
8	22.2	16	54.4	24	133.2	32	326.0

and radiation effects satellite CRRES. This instrument, called MICS/CRRES, was explained in detail by Wilken *et al.* (1992). MICS filters ions with equal value of the energy per charge state E/Q and measures their time-of-flight τ and residual energy E_m. These parameters are then used to determine the ion mass M in amu, charge state Q, and energy E. The energy range from 10.1 to 326.0 keV/e is covered by 32 energy steps (see Table 5). The collimator and the electrostatic analyser have a special toroidal shape that limits the aperture to $\pm 2°$, but provides a relatively large geometric factor of 0.07 cm^2 sr.

MICS produces different kinds of data. This study includes matrix rates (MR), event rates (ER), and direct events (DE). The matrix rates (MR) are obtained as follows: the digital processing unit (DPU) identifies the ions by determining the mass per charge state M/Q and the mass M according to

$$\frac{M}{Q} = 2\frac{E}{Q}\left(\frac{\tau}{d}\right)^2 \tag{1}$$

and

$$M = 2\frac{E_m}{\eta(E_m)}\left(\frac{\tau}{d}\right)^2. \tag{2}$$

$d = 67$ mm is the length of the flightpath; E_m is the residual energy measured by a solid state detector; $\eta(E_m)$ is the correction factor for the energy losses in the dead layer of the solid-state detector. The ions are then fed into a M–M/Q matrix with $16M$ bins and $32M/Q$ bins, having a total of 512 elements. The elements corresponding to a given ion species are taken together as matrix element groups. The contents of these groups are transmitted as matrix rates (MR). The accumulation time of MR is 0.1225 s during each E/Q step of 0.15 s. Since E_m is needed for the ion identification, the MR are restricted to high ion energies. We only used them for H^+ ions with energies above about 35 keV.

The event rates (ER) include the number of start signals for the time-of-flight measurement (FSR), the number of valid pairs of start and stop signals from which the time-of-flight can be determined (DCR), the number of events for which valid time-of-flight and energy measurements are available (TCR), and the number of ions for which the solid state detector measured the ion energy (MSS). The accumulation time is the same as for MR. We used DCR to determine the H^+ ion intensity. Since DCR includes counts from all ion species a correction procedure was developed that is explained below.

The direct events (DE) are obtained from the direct transmission of pairs of time-of-flight (τ) and energy (E_m) measurements for known values of E/Q. The number of direct events is limited to six per E/Q step of 0.15 s. If more events than one occur during each of the six 0.01875-s subintervals, a priority scheme selects the heaviest of these ions. At low energies, at which no measurement of E_m from the solid-state detector is available, τ is transmitted alone. M/Q can still be determined for these ions (see Eq. 1).

τ and E_m are used to investigate the ion composition. For this purpose, τ was plotted versus E/Q (Fig. 4a–e). Curves for $M/Q = 1, 2, 4, 16$ corresponding to H^+, He^{++}, He^+ and O^+ ions indicate the expected locations of the different ion species. The curves are corrected for the ion energy losses in the carbon foil that were calculated by a computer code developed by Ziegler *et al.* (1985). The validity of these curves is verified by the location of high energy ions for which E_m was measured and M could therefore be determined. The He^{++} ion counts in Fig. 5 are derived from DE by selecting all events close to the $M/Q = 2$ curve.

DE is also used to correct DCR for counts that are not due to H^+ ions. This is achieved by subtracting from DCR the sum of all counts outside a region close to the curve for $M/Q = 1$. The correction is almost negligible in the ring current where DCR is much larger than the sum of the DE. It is important, however, close to the cusp where DCR is also small. The validity of this procedure was tested by comparing the energy spectra for the corrected DCR with the MR for H^+ in Fig. 8. The intensities obtained from MR practically coincide with those obtained from the corrected DCR in the energy range for which the MR are available. We therefore regard the corrected values of DCR as the number of H^+ counts even at lower energies.

A special effort is needed for the identification of heavy high-charge state ions. These ions suffer strong energy losses in the carbon foil and in the dead layer of the solid-state detector that depend on the ion species. We had available model calculations for the energy losses of carbon, nitrogen, oxygen and argon and used them to correct the energy values measured by the solid state detector. $E_{corr} = E_m/\eta(E_m)$ and τ then provide M according to Eq. (2). Q can be determined from E_{corr} and the

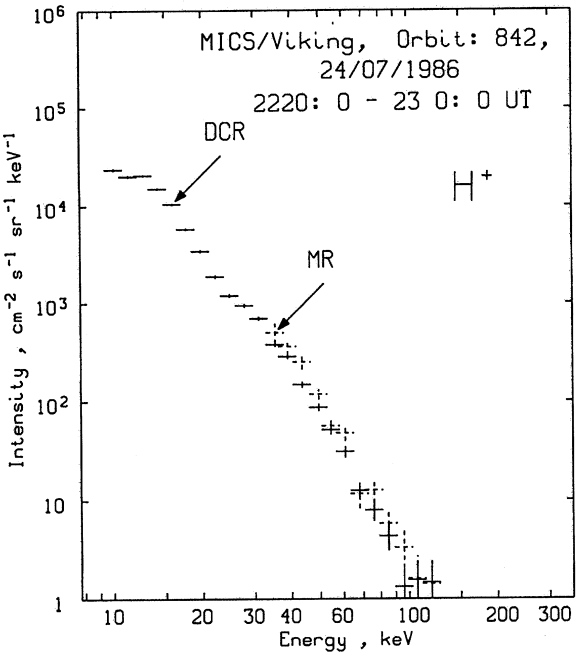

Fig. 8. A comparison of the energy spectra of the H^+ ion intensity obtained from two different data origins. The terms DCR and MR are explained in the text

known values of E/Q. This method is reliable for most of the carbon and oxygen ions. In some cases the values of M/Q were used to distinguish between different identification possibilities, since M/Q is calculated from E/Q (Eq. 1) and is therefore more reliable than M. For the ions heavier than oxygen we assumed in advance that these are solar wind ions. In case of ambiguities we selected those ion species that could be expected to be present according to measurements with the solar wind ion composition spectrometer SWICS on the space probe ULYSSES (Gloeckler *et al.*, 1992).

Acknowledgements. The magnetic field measurements on Viking from which the pitch angles were calculated were provided by T. Potemra, Applied Physics Laboratory, John Hopkins University, Laurel, MD, USA. The ion energy losses in the carbon foil and the solid state detector were calculated by G. Kettmann, Max-Planck-Institut für Aeronomie, Katlenburg-Lindau, Germany. The Viking trajectory was determined by a program developed by K. Stasiewicz, Swedish Institute of Space Physics, Uppsala, Sweden. The transformation of the raw data was performed using programs developed by F. Both, Max-Planck-Institut für Aeronomie, Katlenburg-Lindau, Germany. R. Rasinkangas, University of Oulu, Finland, installed the raw data analysis programs in the central computer of the University of Oulu on which the data analysis has been performed. The MICS/Viking instrument was designed and manufactured in a joint effort between the Max-Planck-Institut für Aeronomie, Germany; the Aerospace Corporation, USA; the Rutherford-Appleton Laboratory, UK; and the University of Bergen, Norway. The Viking project was managed and operated by the Swedish Space Corporation under contract from the Swedish Board for Space Activities.

Topical Editor C.-G. Fälthammar thanks F. Söraas and A.D. Johnstone for their help in evaluating this paper.

References

Amundsen, R., F. Søraas, and K. Aarsnes, Cleft signature in proton fluxes above 100 keV, *J. Geophys. Res.*, **80,** 685–689, 1975.

Anagnostopoulos, G. C., and G. D. Kaliabetsos, Shock drift acceleration of energetic ($E \geq 50$ keV) protons and ($E \geq 37$ keV) alpha particles at the Earth's bowshock as a source of the magnetosheath energetic ion events, *J. Geophys. Res.*, **99,** 2335–2349, 1994.

André, M., H. Koskinen, L. Matson, and R. Erlandson, Local transverse ion energization in and near the polar cusp, *Geophys. Res. Lett.*, **15,** 107–110, 1988.

André, M., G. B. Crew, W. K. Peterson, A. M. Persoon, J. C. Pollock, and M. J. Engebretson, Ion heating by broadband low-frequency waves in the cusp/cleft, *J. Geophys. Res.*, **95,** 20809–20823, 1990.

Aparicio, B., B. Thelin, and R. Lundin, The polar cusp from a particle point of view: A statistical study based on Viking data, *J. Geophys. Res.*, **96,** 14023–14031, 1991.

Burch, J. L., P. H. Reiff, R. A. Heelis, J. D. Winningham, W. B. Hanson, C. Gurgiolo, J. D. Menietti, R. A. Hoffman, and J. N. Barfield, Plasma injection and transport in the mid-altitude polar cusp, *Geophys. Res. Lett.*, **9,** 921–924, 1982.

Delcourt, D. C., J. A. Sauvaud, and T. E. Moore, Cleft contribution to ring current formation, *J. Geophys. Res.*, **95,** 20937–20943, 1990.

Gloeckler, G., J. Geiss, H. Balsiger, P. Bedini, J. C. Cain, J. Fischer, L. A. Fisk, A. B. Galvin, F. Gliem, D. C. Hamilton, J. V. Hollweg, F. M. Ipavich, R. Joos, S. Livi, R. Lundgren, U. Mall, J. F. McKenzie, K. W. Ogilvie, F. Ottens, W. Rieck, E. O. Tums, R. von Steiger, W. Weiss, and B. Wilken, The solar wind ion composition spectrometer, *Astron. Astrophys. Suppl. Ser.*, **92,** 267–289, 1992.

Hultqvist, B., The Viking project, *Geophys. Res. Lett.*, **14,** 379–382, 1987.

Hultqvist, B., The Swedish satellite project Viking, *J. Geophys. Res.*, **95,** 5749–5752, 1990.

Kremser, G., and R. Lundin, Average spatial distributions of energetic particles in the midaltitude cusp/cleft region observed by Viking, *J. Geophys. Res.*, **95,** 5753–5766, 1990.

Kremser, G., W. Stüdemann, B. Wilken, G. Gloeckler, D. C. Hamilton, and F. M. Ipavich, Average spatial distributions of energetic O^+, O^{2+}, O^{6+}, and C^{6+} ions in the magnetosphere observed by AMPTE/CCE, *J. Geophys. Res.*, **92,** 4459–4466, 1987.

Lockwood, M., and M. F. Smith, The variation of reconnection rate at the dayside magnetopause and cusp precipitation, *J. Geophys. Res.*, **97,** 14841–14847, 1992.

Lockwood, M., M. O. Chandler, J. L. Horwitz, J. H. Waite, Jr., T. E. Moore, and C. R. Chappell, The cleft ion fountain, *J. Geophys. Res.*, **90,** 9736–9748, 1985.

Lyons, L. R., Vampola, A. L., and T. W. Speiser, Ion precipitation from the magnetopause current sheet, *J. Geophys. Res.*, **92,** 6147–6151, 1987.

Newell, P. T., and C.-I. Meng, The cusp and the cleft/boundary layer: Low-altitude identification and statistical local time variation, *J. Geophys. Res.*, **93,** 14549–14556, 1988.

Peterson, W. K., T. Abe, M. André, M. J. Engebretson, H. Fukunishi, H. Hayakawa, A. Matsuoka, T. Mukai, A. M. Persoon, J. M. Retterer, R. M. Robinson, M. Sugiura, K. Tsuruda, D. D. Wallis, and A. W. Yau, Observations of a transverse magnetic field perturbation at two altitudes on the equatorward edge of the magnetospheric cusp, *J. Geophys. Res.*, **98,** 21463–21470, 1993.

Rasinkangas, R., G. Kremser, B. Wilken, and F. Søraas, Substorm related energy-latitude dispersion of energetic ions in the dayside magnetosphere: Viking observations, *Ann. Geophysicae*, **9,** 628–639, 1991.

Sandahl, I., R. Lundin, and L. Eliasson, The hot plasma spectrometers on Viking, *KGI report 077*, Swedish Institute of Space Physics, Kiruna, Sweden, 1985.

Stadsnes, R., Presentasjon av data fra Viking-satellitten, *M.Sc. Thesis*, University of Bergen, Department of Physics, Bergen, Norway, 1988.

Stüdemann, W., and B. Wilken, Detection efficiency of a heavy ion time-of-flight spectrometer with thin carbon foils in the start detector, *Rev. Sci. Instrum.*, **53,** 175–180, 1982.

Stüdemann, W., B. Wilken, G. Kremser, A. Korth, J. F. Fennell, B. Blake, R. Koga, D. Hall, D. Bryant, F. Søraas, K. Brønstad,

T. A. Fritz, R. Lundin, and G. Gloeckler, The May 2–3, 1986 magnetic storm: First energetic ion composition observations with the MICS instrument on VIKING, *Geophys. Res. Lett.*, **14,** 455–458, 1987.

Thelin, B., B. Aparicio, and R. Lundin, Observations of upflowing ionospheric ions in the mid-altitude cusp/cleft region with the Viking satellite, *J. Geophys. Res.*, **95,** 5931–5939, 1990.

Watermann, J., O. de la Beaujardière, D. Lummerzheim, J. Woch, P. T. Newell, T. A. Potemra, F. J. Rich, and M. Shapshak, The dynamic cusp at low altitudes: A case study combining Viking, DMSP-F7, and Sondrestrom incoherent scatter radar observations, *Ann. Geophysicae*, **12,** 1144–1157, 1994.

Wilken, B., W. Weiß, D. Hall, M. Grande, F. Søraas, and J. F. Fennell, Magnetospheric ion composition spectrometer onboard the CRRES spacecraft, *J. Spacecr. Rockets*, **29,** 585–591, 1992.

Winglee, R. M., J. D. Menietti, W. K. Peterson, J. L. Burch, J. H. Waite, Jr., and B. Giles, Magnetosheath-ionospheric plasma interactions in the cusp/cleft, 1. Observations of modulated injections and upwelling ion fluxes, *J. Geophys. Res.*, **98,** 19315–19329, 1993.

Woch, J., and R. Lundin, Magnetosheath plasma precipitation in the polar cusp and its control by the interplanetary magnetic field, *J. Geophys. Res.*, **97,** 1421–1430, 1992.

Yau, A. W., B. A. Whalen, W. K. Peterson, and E. G. Shelley, Distribution of upflowing ionospheric ions in the high-altitude polar cap and auroral ionosphere, *J. Geophys. Res.*, **89,** 5507–5522, 1984.

Ziegler, J. F., J. P. Biersack, and U. Littmark, "*The stopping and range of ions in solids*", Pergamon Press, New York, 1985.